AIAA JOURNAL
Vol. 30, No. 3, March 1992

Experimental Investigation of the Perpendicular Rotor Blade-Vortex Interaction at Transonic Speeds

Iraj M. Kalkhoran*
Polytechnic University, Farmingdale, New York 11735
and
Donald R. Wilson† and Donald D. Seath†
University of Texas at Arlington, Arlington, Texas 76019

Transonic perpendicular rotor blade-vortex interaction (BVI) tests at Mach numbers ranging from 0.68 to 0.9 and Reynolds numbers (based on the airfoil chord) of 3.8–5.5 million were conducted in the UTA high-Reynolds number, transonic Ludwieg-tube wind tunnel. The scheme involved positioning a lifting wing (vortex generator) upstream of an instrumented NACA 0012 airfoil so that the trailing vortex interacted with the downstream airfoil. Tests were performed at several vortex strengths as well as several vortex core heights above the downstream airfoil. The results obtained from these experiments indicate that a substantial change in the pressure distribution of the downstream airfoil occurs, but most of the effects were confined to the leading 30% of the airfoil chord. A spanwise drift of the vortex core as it passes over the trailing airfoil, similar to results observed previously in low-speed wind tunnel tests, as well as a high degree of unsteadiness in the vicinity of the vortex center were observed.

Nomenclature

AR = aspect ratio
b = span
C_D = drag coefficient
C_L = lift coefficient
C_p = pressure coefficient
C_p^* = critical pressure coefficient
c = airfoil chord
d = vortex core diameter
h = vortex height above the airfoil
M = Mach number
p = pressure
Re = Reynolds number
S = planform area
s = spanwise drift of vortex center
t = time
V = velocity
x, y, z = Cartesian coordinates
α = angle of attack
Γ = circulation
γ = specific heat ratio

Subscripts

t = total
v = vortex core
VG = vortex generator
∞ = free stream

Introduction

A THOROUGH physical understanding of the blade-vortex interaction (BVI) phenomena is necessary for the development of high-performance helicopter rotors. Not only does the trailing vortex system shed from one blade of a helicopter rotor exert a significant influence on the aerodynamic characteristics of the following blades,[1-3] but in addition, the blade-vortex interaction has been identified as the primary mechanism involved in the acoustic phenomenon known as "blade slap."[4-6]

In general, the rotor blade-vortex interaction is a highly three-dimensional, unsteady interaction of curved vortices with lifting surfaces at arbitrary interaction angles. The limiting cases for the interaction angles are represented by the parallel and perpendicular encounters, as shown in Fig. 1 (from Ref. 7). The parallel interaction is essentially two-dimensional but highly unsteady, while the perpendicular interaction is a steady but highly three-dimensional flow. Under certain flight conditions, rotor blades operating at transonic relative tip Mach numbers produce impulsive noise at a frequency approximately corresponding to the blade passage frequency. The impulsive noise generated by the BVI phenomenon is known to be a result of the rapid load variations caused by a rotor blade passing close to or through a tip vortex generated by the same or one of the following blades. Moreover, at transonic Mach numbers, unsteady shock formation and pressure fluctuations play an important role in the generation of "blade-slap." The aeroacoustic implications of blade-vortex interactions are covered in papers by George,[8] George and Chang,[9] and more recently by Leverton.[10] The noise produced by interaction of vortices with lifting surfaces is not limited to the main rotor. In fact, it has been shown that the noise associated with the interaction between the main rotor vortex and the tail rotor can be subjectively annoying, and in certain operating conditions can dominate both the main rotor BVI noise as well as the engine noise.[11]

The BVI problem has been the subject of extensive investigations during the past few years. Although the normal operating envelope for helicopter rotor blades is at transonic relative Mach numbers, most of the experimental research in this area has concentrated on the low speed interaction.[1,12] The limited high speed data available deal exclusively with the unsteady parallel BVI phenomenon (e.g. Refs. 13, 14); because this encounter, due to its unsteady nature, is believed to be the main source for the noise. Among the relevant investigations of the perpendicular interaction are those due to Schlinker and Amiet,[15] who conducted three-dimensional

Presented as Paper 87-0208 at the AIAA 25th Aerospace Sciences Meeting, Reno, NV, Jan. 12–15, 1987; received Feb. 7, 1991; revision received July 3, 1991; accepted for publication July 21, 1991.

*Assistant Professor, Aerospace Engineering Department. Member AIAA.
†Professor, Department of Aerospace Engineering. Associate Fellow AIAA.

interaction experiments using hot wire measurements in the vortex core to determine the acoustic signature. They concluded that ingestion of the vortex by the rotor generates harmonic noise and impulsive wave forms. Ham[12] conducted detailed aerodynamic investigations of the perpendicular vortex-airfoil interaction and measured lift coefficient variations of 0.2 to 0.3. He also observed the occurrence of flow separation induced by intensive vortex loading. Phillipe and Armand[16] observed a 40% increase in drag and a loss of lift for a NACA 0012 airfoil at $M = 0.6$. Low-speed experimental studies of Seath and Wilson[1] also indicated a significant change in the pressure distribution of the interacting airfoil, as well as a spanwise drift to the vortex resulting from the perpendicular vortex-airfoil interaction.

A simple dimensional analysis of the perpendicular blade-vortex interaction problem indicates that the governing simulation parameters are the rotor Mach number, Reynolds number, and angle of attack; a vortex interaction parameter defined by $\Gamma/V_\infty c$, where Γ is the vortex circulation, V_∞ the rotor relative velocity, and c the rotor chord; and the pertinent geometric parameters describing the position of the vortex core with respect to the trailing rotor blade. The specific objectives of the research program reported in this paper were to develop experimental procedures and techniques for simulation of the perpendicular helicopter rotor blade-vortex interaction (BVI) in a Ludwieg-tube wind tunnel at Mach numbers and Reynolds numbers representative of operational advancing rotor blade flight conditions, and to quantify the effects of vortex strength and height on both the structure of the vortex as it passes over the rotor and the aerodynamic characteristics of the rotor blade. Similar results from low-speed wind tunnel tests were reported in Ref. 1.

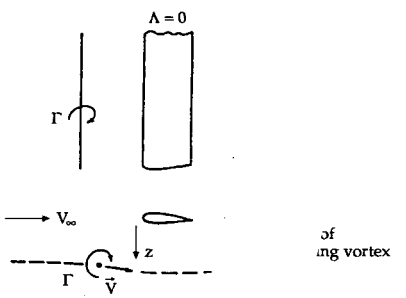

a) Vortex parallel edge

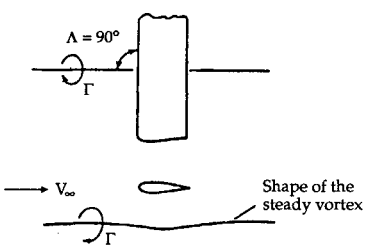

b) Vortex parallel to free stream

Fig. 1 Parallel and perpendicular blade-vortex interactions (from Ref. 7).

Experimental Setup

The UTA high Reynolds number transonic wind tunnel (Fig. 2) is a Ludwieg-tube tunnel designed to provide high Reynolds number transonic flows.[17,18] Maximum steady-state stagnation pressures of about 3.8×10^6 N/m^2 (550 psia) can be generated, giving unit Reynolds numbers of up to 8×10^8 per meter (20 million per in.). The tunnel has an 18.6 × 23.3 cm (7.34 × 9.16 in.) rectangular, porous-wall test section. The variable porosity is provided for all four walls and was set to a predetermined value of 7% for the tests reported in this paper.

Facility operation and control, data acquisition, and data processing were accomplished by a custom-designed microcomputer-based data acquisition system. A schematic of the system is shown in Fig. 3. The data acquisition/control computer (DAC) controls the operation of the tunnel, collects data from a 24-channel high-frequency pressure transducer system, digitizes the data and stores it in memory during a test run. The stored data are then transferred to the host computer for permanent storage on disk and subsequent data reduction and analysis after completion of the test run.

The test geometry for the experimental simulation of the perpendicular blade-vortex interaction is shown in Fig. 4. An instrumented NACA 0012 airfoil, spanning the entire height of the test section, was mounted 43.18 cm (17 in.) downstream of the test section entrance. The downstream airfoil was equipped with 12 static pressure ports on the upper surface. The chordwise location of the orifices are tabulated in Table 1. The pressure tubes were 1.14 mm (0.045 in.) i.d. with six 0.51 mm (0.02 in.) diameter feeder holes each, which results in averaging the chordwise pressure distribution along a 2.54 (1 in.) span of the airfoil at the midspan position. The airfoil had a 5.08 cm (2 in.) chord and was set 1.93 cm (0.75 in.) off centerline, with the uninstrumented surface closer to the test section wall. The model blockage was approximately 3.2%.

For the interaction studies, the vortex was generated by horizontally mounted semispan wing sections, having a 5.08 cm (2 in.) chord and located at the entrance to the test section, which was approximately nine chord lengths upstream of the test airfoil. The distance from the vortex core to the airfoil surface was varied by using three different vortex-generators with semispans of 12.95 cm, 13.46 cm, and 13.97 cm (5.1 in., 5.3 in., and 5.5 in.). This resulted in vortex heights (h/c)

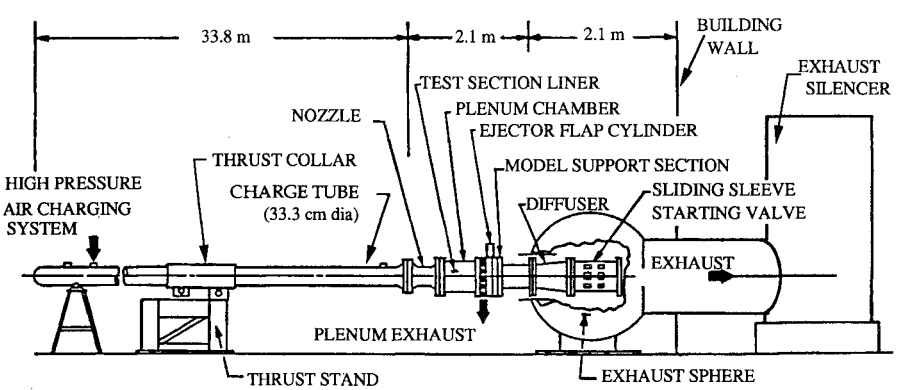

Fig. 2 Transonic Ludwieg-tube wind tunnel.

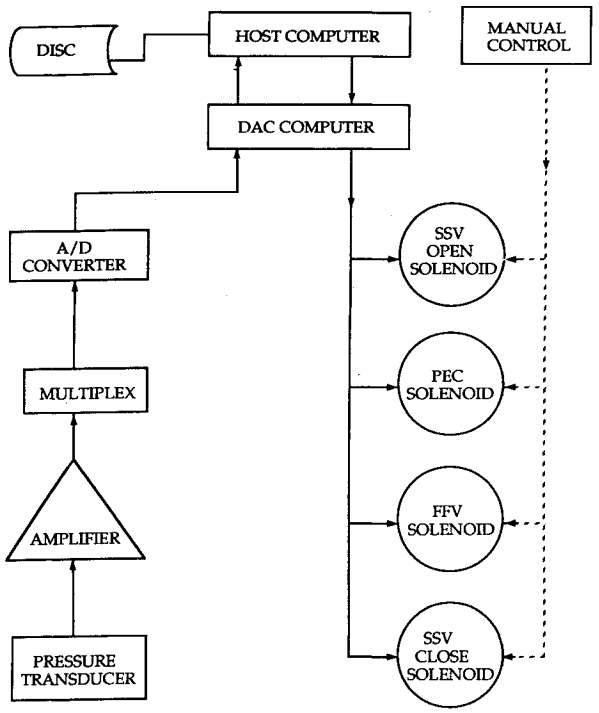

Fig. 3 Facility control and data acquisition system.

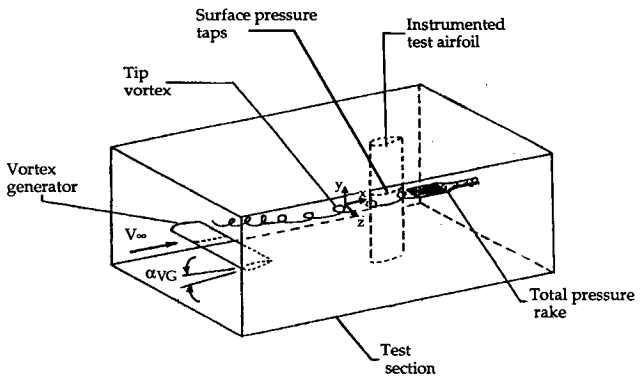

Fig. 4 Simulation of perpendicular blade-vortex interaction.

Table 1 Port locations and airfoil thickness for the NACA 0012 airfoil section

Port number	X/C	Y/C
1	0.025	0.026
2	0.10	0.047
3	0.15	0.053
4	0.20	0.057
5	0.30	0.060
6	0.40	0.058
7	0.50	0.053
8	0.55	0.050
9	0.60	0.046
10	0.65	0.041
11	0.75	0.032
12	0.80	0.026

measured at the airfoil leading edge of 30%, 20%, and 10% chord above the airfoil. The vortex strength was varied by pitching the vortex generator to different angles of attack. The aerodynamic characteristics of the vortex generators were determined by mounting the generators to a five-component strain-gage balance that could be inserted through an optical port in the test section side wall.

The location and detailed qualitative structure of the tip vortices were determined by means of a pitot pressure rake and a five-hole cone probe. The pitot pressure rake contained 13 pressure probes with 0.32 cm (0.125 in.) spacing. The five-hold cone probe had a total pressure orifice at the nose and four equally spaced ports on the cone surface. This probe was used primarily to verify the data obtained using the pitot pressure rake and to obtain information concerning the vortex viscous core size and symmetry.

Uncertainty Analysis

The results of a conventional uncertainty analysis were reported in detail in Ref. 18. For the range of data reported in this paper, the typical values of the uncertainty in the principal test variables are:

$$M_\infty : 0.015-0.018$$

$$Re : 1.4-1.6(10)^5$$

$$p_t/p_{t\infty} : 0.01-0.012$$

$$C_p : 0.03-0.06$$

Wind Tunnel Calibration

Standard wind tunnel calibration tests were conducted at Mach numbers ranging from 0.68 to 0.90 and Reynolds numbers from 3.8 to 5.5 million. The results of the calibration tests and flow quality and uniformity studies for the Ludwieg-tube tunnel may be found in Ref. 18. In general, the flow quality is quite good, with the axial Mach number variation less than $\pm 0.5\%$ for the range of Mach numbers tested. Furthermore, the background noise level (as indicated by rms surface pressure fluctuation measurements) is less than 1.0%.

Airfoil Calibration

The airfoil calibration tests for a range of Mach and Reynolds numbers were conducted prior to the initiation of the blade-vortex interaction tests. The major objectives of this phase of the program were the production of baseline airfoil pressure distribution data for the subsequent interaction studies, and the determination of the accuracy and repeatability of the test data. Figure 5 illustrates a comparison between the results of the current study and the data of Ref. 19. Considering the small difference in the indicated angles of attack and the different wind tunnel blockage factors, the agreement is quite good. Repeatability of the airfoil pressure distribution data for the Ludwieg-tube tunnel is illustrated in Fig. 6, where the surface pressure distributions from three different runs at essentially identical test conditions are compared to the data of Ref. 20. The results of a comprehensive study of the airfoil

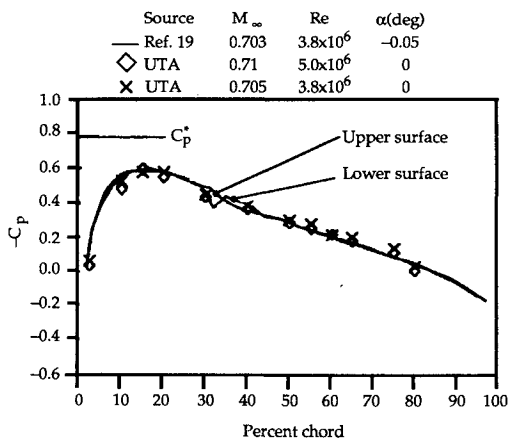

Fig. 5 Comparison of measured upper surface pressure distribution with data of Ref. 19.

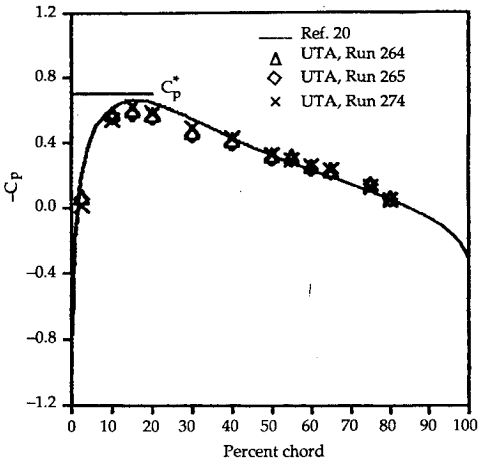

Fig. 6 Repeatability of pressure distribution data: $M_\infty = 0.72$, $Re = 5.1 \times 10^6$.

pressure distribution for a range of Mach and Reynolds numbers may also be found in Ref. 18.

Vortex Generator Aerodynamic Characteristics

An important dimensionless parameter characterizing the BVI is the vortex interaction parameter $\Gamma/V_\infty c$, where Γ is the vortex circulation, and is defined by

$$\Gamma = \oint V \cdot d\mathbf{r} \tag{1}$$

In general, the circulation Γ is a difficult and time-consuming parameter to measure experimentally. For this reason, the lift coefficient of the vortex generator is often used as an alternate parameter to characterize the vortex. Note that from classical low-speed aerodynamic theory,[21] the lift of a finite wing with an elliptic spanwise circulation distribution is given by

$$L = \int_{-b/2}^{+b/2} \rho_\infty V_\infty \Gamma_o \sqrt{1 - \left(\frac{y}{b/2}\right)^2}\, dy$$

$$= \frac{\pi}{4} b \rho_\infty V_\infty \Gamma_o \tag{2}$$

Thus, the lift coefficient for the elliptic distribution

$$C_L = \frac{L}{\frac{1}{2}\rho_\infty V_\infty^2 S} = \frac{\pi b \Gamma_o}{2 V_\infty S} \tag{3}$$

is seen to be directly proportional to the maximum, or midspan, circulation Γ_o. Of course, Eq. (3) is not expected to be quantitatively correct for the rectangular planform used in the current test program, however, the functional form indicated by Eq. (3) should remain valid, that is:

$$C_L \sim \frac{b\Gamma_o}{V_\infty S} \sim \frac{b\Gamma_o}{V_\infty b c} \sim \frac{\Gamma_o}{V_\infty c} \tag{4}$$

Thus, as a data correlation parameter, C_L should be just as valid as $\Gamma/V_\infty c$. Therefore, a test program was conducted to measure the aerodynamic characteristics of the vortex generator wings (C_L and C_D vs α), and typical results are shown in Fig. 7.

Vortex Survey

The vortex core geometric position, i.e. the location of the vortex core above the airfoil z_v and along the span y_v, was

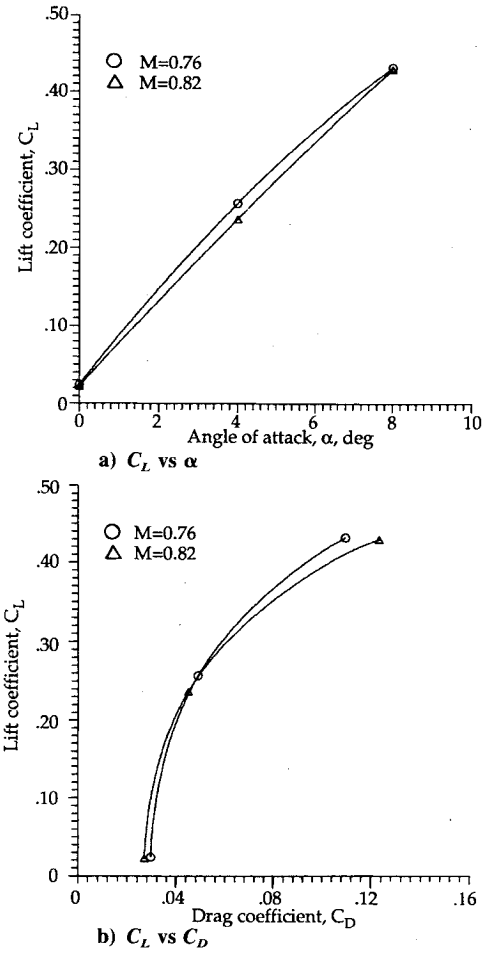

Fig. 7 Aerodynamic characteristics of vortex generator, $AR = 5.1$.

measured by a pitot pressure rake located approximately nine chord lengths downstream of the vortex generator, with the probes spanning a segment of the flow in the z direction (Fig. 4). Two-dimensional mapping of the vortex was then accomplished by positioning the rake at different spanwise positions for subsequent wind tunnel firings. Typical results from the pitot pressure rake survey of the vortex structure are shown in Fig. 8. Figure 8a shows a horizontal pressure survey through the core of the vortex at different times during the steady-state part of the test run. Two points are immediately obvious. First, the vortex seems to have a well-defined core, with the pressure deficits in the core region on the order of 20% to 25% of the test-section stagnation pressure. Second, the results of the rake survey indicate a substantial amount of unsteadiness near the vortex center. Selected pressure vs time traces are shown in Fig. 8b for various probe locations. These traces (obtained by scanning the pressure transducer output at 1 ms time intervals) show considerable pressure fluctuations near the center of the vortex (defined to be the minimum total pressure location); however, these fluctuations tend to damp out at distances further away from the vortex center. The fluctuations in pressure are thought to be a result of oscillation of the vortex core about a mean position. Time-mean averaging of the pressure traces (after completion of the tunnel starting transient) gives a steady mean value, and these data have been used to generate the constant pressure contour map of Fig. 9. The projection of the vortex generator quarter-chord line is shown as the dashed line in Fig. 9. The vortex in-board roll-up as well as the influence of the upwash field (the vortex generator was set to a negative angle of incidence) is clearly evident.

In order to obtain information concerning the vortex symmetry and its viscous core size (d/c), five-hole cone probe

surveys through the vortex core were also conducted. Figure 10 is produced by differencing the pressures of the two opposing ports on the surface of the cone probe. A fairly symmetric vortex structure with a well-defined core can be seen in this figure. The nondimensional viscous core diameter is approximately 0.25 (d/c = 0.25).

Blade-Vortex Interaction

The blade-vortex interaction measurements were primarily in the form of pressure distribution changes on the upper surface of the test (downstream) airfoil. The generated vortex always passed over the instrumented surface of the downstream airfoil. The effect of vortex strength on the pressure distribution of the airfoil is illustrated in Fig. 11a, where the results obtained from three different vortex generator angles of attack are compared to the vortex-free pressure distribution for a freestream Mach number of 0.70. This Mach number corresponds to a subcritical flow over the airfoil. A substantial change in the pressure distribution near the leading edge of the airfoil, where the vortex-induced pressure gradient normal to the airfoil surface is the greatest, is quite evident. The effect of the vortex tends to damp out downstream of the minimum C_p location and the pressure distribution is dominated by the vortex-free mean flow. One possible explanation for this behavior is the spanwise drift of the vortex after interacting with the downstream airfoil, which is discussed in the following section. The effect of the interacting airfoil on the structure of the vortex is also of vital importance in the analysis of the vortex-airfoil interaction. Phenomena such as vortex diffusion and breakdown, particularly at closer encounters, may also be responsible for weakening of the vortex influence on the pressure distribution of the interacting airfoil beyond x/c = 0.30. The vortex breakdown and flow separation phenomenon have been observed by flow visualization techniques for similar interaction problems by several investigators (e.g., Ref. 22). Figures 11b and 11c indicate the same trend for freestream Mach numbers of 0.74 and 0.78, which correspond to supercritical flows over the airfoil. A more pronounced change in the pressure distribution of the downstream airfoil is observed when the airfoil is set to a 2-deg angle of attack (Fig. 11d). Locally vortex-induced supersonic and separated flow regions near the airfoil leading edge (x/c = 0.025) are shown in Fig. 11d.

In order to determine the effect of the vortex height above the airfoil, tests were conducted using three vortex generator semispans that yield vortex heights of 10%, 20%, and 30% of the airfoil chord, as measured at the airfoil leading edge. These results are shown in Fig. 12, where a progressive increase in the magnitude of the pressure coefficient near the leading edge is observed as the vortex height above the upper surface of the airfoil is reduced. Also evidence of local flow separation near the x/c = 0.70 position is observed for the closer encounters.

The change in pressure coefficient near the leading edge is plotted vs lift coefficient of the vortex generator for vortex heights of 0.1, 0.2, and 0.3 in Fig. 13 for a Mach number of 0.76. Note from our earlier discussion, this plot in effect shows the influence of vortex interaction parameter and h/c on the maximum change in C_p. The effect is quite pronounced, with the maximum ΔC_p of 0.48 occurring for the combination of the strongest vortex, C_L = 0.432, and the closest encounter, h/c = 0.1. Note that although the method used to vary vortex height does cause a slight change in aspect ratio of the vortex generator (~7%), the effect of this variation on C_L was analyzed and found to be negligible.

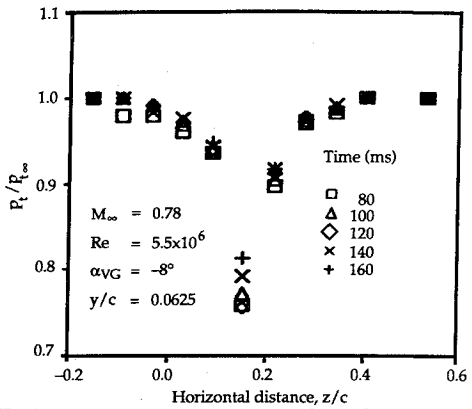

a) Horizontal total pressure survey through vortex core

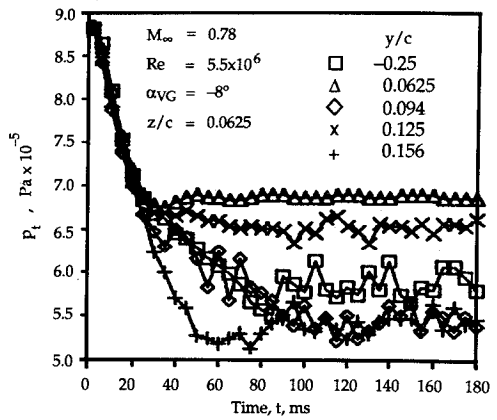

b) Total pressure vs time at selected vertical locations

Fig. 8 Vortex survey: M_∞ = 0.78, Re = 5.5 × 10⁶, α_{VG} = −8 deg.

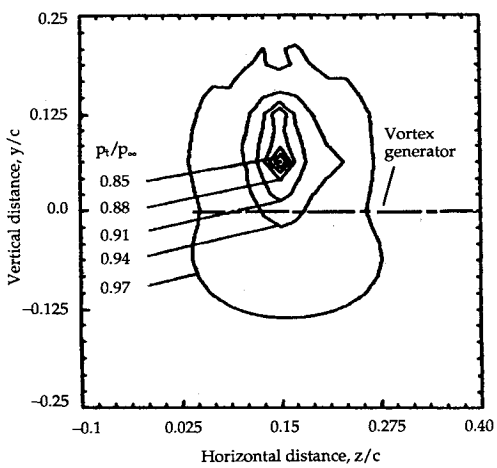

Fig. 9 Time-averaged total pressure contour map: M_∞ = 0.78, Re = 5.5 × 10⁶, α_{VG} = −8 deg.

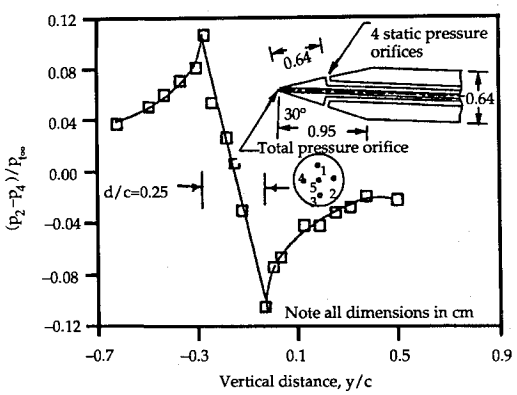

Fig. 10 Five-hold cone probe survey of vortex viscous core: M_∞ = 0.75, Re = 5.4 × 10⁶, α_{VG} = −8 deg.

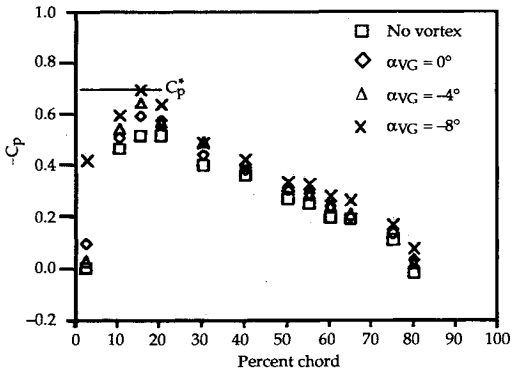

a) Airfoil angle of attack of 0 deg: $M_\infty = 0.70$, $Re = 5.1 \times 10^6$, $h/c = 0.1$

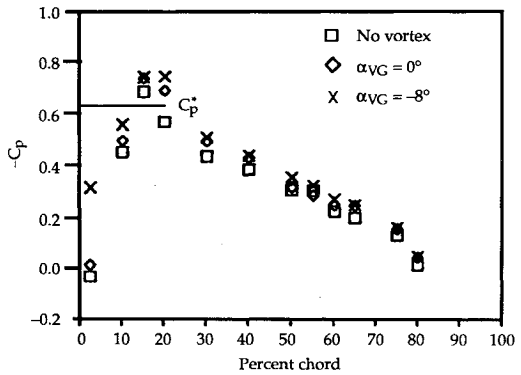

b) Airfoil angle of attack of 0 deg: $M_\infty = 0.74$, $Re = 5.2 \times 10^6$, $h/c = 0.1$

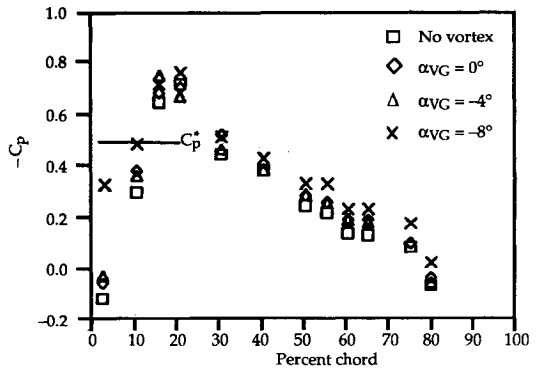

c) Airfoil angle of attack of 0 deg: $M_\infty = 0.78$, $Re = 5.4 \times 10^6$, $h/c = 0.1$

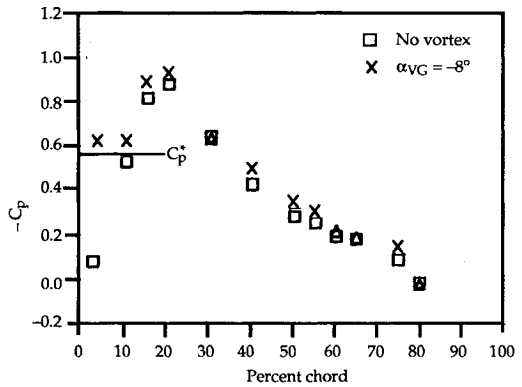

d) Airfoil angle of attack of 2 deg: $M_\infty = 0.76$, $Re = 5.4 \times 10^6$, $h/c = 0.1$

Fig. 11 Effect of vortex strength on airfoil pressure distribution.

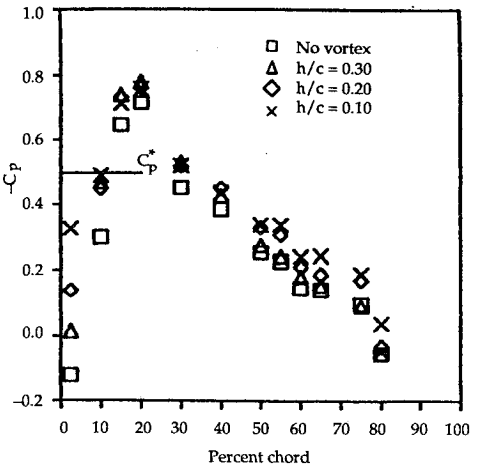

Fig. 12 Effect of vertical height of vortex core above airfoil surface: Airfoil angle of attack of 0 deg $M_\infty = 0.78$, $Re = 5.5 \times 10^6$, $\alpha_{VG} = -8$ deg.

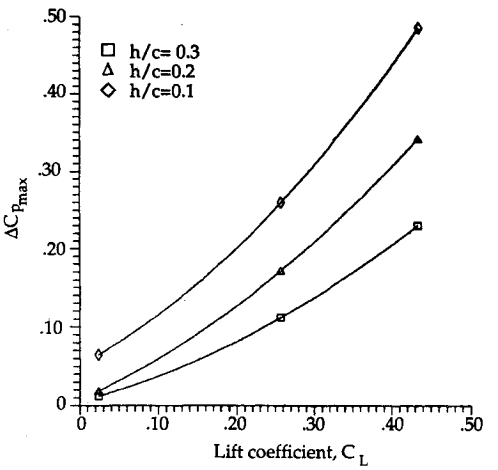

Fig. 13 Effect of vortex strength and vortex height on $\Delta C_{P\max}$: $M = 0.76$, $Re = 5.3 \times 10^6$.

The aforementioned results discussed for typical vortex strengths and heights above the airfoil are qualitatively similar for all Mach and Reynolds numbers tested throughout this study.

The variation of Reynolds number, as shown in Fig. 14, does not seem to have a significant effect on the pressure distribution of the downstream airfoil, for the range of Reynolds numbers (3.8–5.5 million) tested during this program.

Structure of the Vortex

The structure of the vortex after interacting with the airfoil was qualitatively examined by conducting total pressure rake surveys at both the leading and the trailing edges of the downstream airfoil. Figure 15 shows the results of typical rake surveys through the vortex center at both the leading and trailing edges for a vortex core height (h/c) of 0.20. The unsteady nature of the flow in the vicinity of the vortex center, similar to that observed in Fig. 8 for the free vortex, is clearly evident in Fig. 15 also.

Time-mean average pitot pressure contour maps of the vortex at the airfoil leading and trailing edges are shown in Fig. 16 for $h/c = 0.30$. Similar contour maps for vortex heights of 20% and 10% at the airfoil leading and trailing edges are shown in Figs. 17 and 18, respectively. For the case of the closest encounter ($h/c = 0.10$) the interaction between the vortex core and the airfoil wake is quite strong (Fig. 18b), but due to the narrow size of the airfoil wake, the vortex is

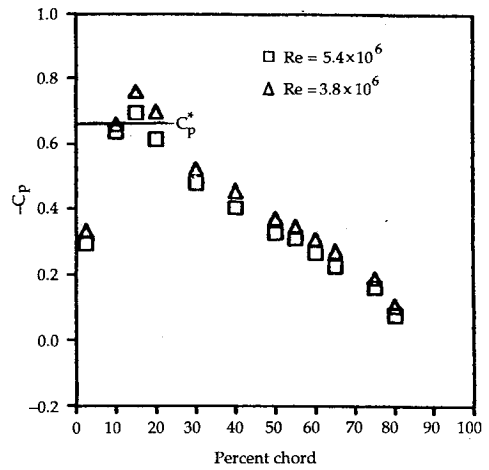

Fig. 14 Effect of Reynolds number variation: $M_\infty = 0.78$, $\alpha_{VG} = -8$ deg, $h/c = 0.20$.

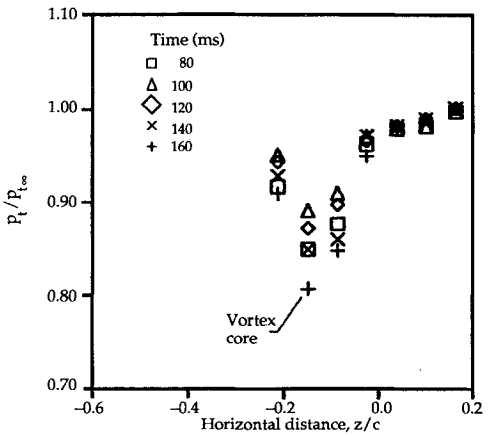

a) Total pressure survey at leading edge

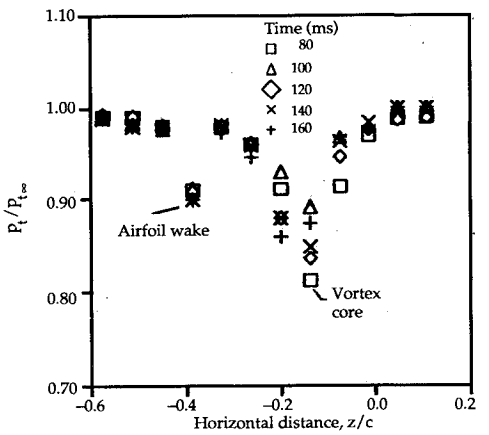

b) Total pressure survey at trailing edge

Fig. 15 Vortex structure in the local vicinity of the airfoil: $\alpha_{VG} = -8$ deg, $h/c = 0.2$, $M_\infty = 0.76$, $Re = 5.4 \times 10^6$.

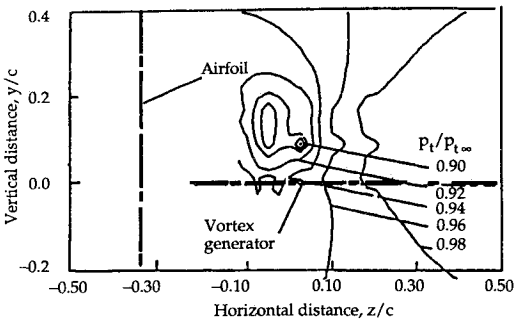

a) Vortex survey at leading edge

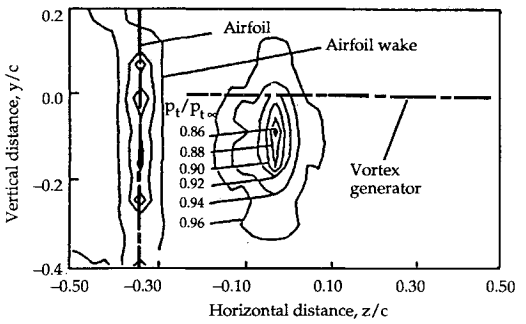

b) Vortex survey at trailing edge

Fig. 16 Time-averaged total pressure contour maps at leading and trailing edges: $\alpha_{VG} = -8$ deg, $h/c = 0.3$, $M_\infty = 0.72$, $Re = 5.1 \times 10^6$.

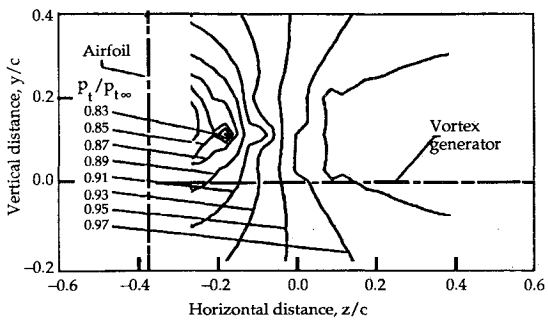

a) Vortex survey at leading edge

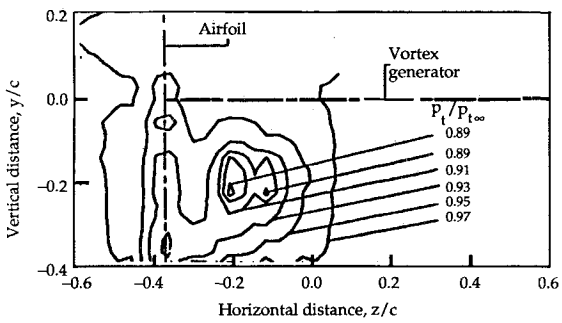

b) Vortex survey at trailing edge

Fig. 17 Time-averaged total pressure contour maps at leading and trailing edges: $\alpha_{VG} = -8$ deg, $h/c = 0.2$, $M_\infty = 0.72$, $Re = 5.1 \times 10^6$.

easily distinguished by its wider band. The contour maps shown in Figs. 16–18 are qualitatively similar to the low-speed test results reported in Ref. 1, and a strong spanwise deflection of the vortex is observed as the vortex passes over the airfoil. An explanation of this behavior based on an image vortex analogy is presented in Ref. 1.

An examination of the contour maps at the trailing edge of the airfoil indicates an increase in the spanwise deflection of the vortex core, as the height of the vortex above the airfoil is reduced. This effect is illustrated in Fig. 19, which presents the measured spanwise drift of the vortex core as a function of the vortex height at the leading edge. Similar results were presented in Ref. 1 for low-speed tunnel simulation of the blade-vortex interaction; however, the magnitude of the drift for the low-speed cases is considerably smaller.

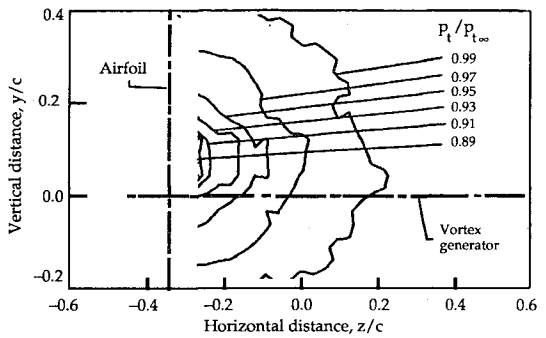

a) Vortex survey at leading edge

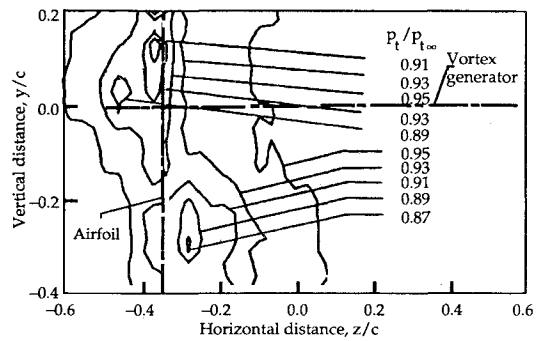

b) Vortex survey at trailing edge

Fig. 18 Time-averaged total pressure contour maps at leading and trailing edges: $\alpha_{VG} = -8$ deg, $h/c = 0.1$, $M_\infty = 0.72$, $Re = 5.1 \times 10^6$.

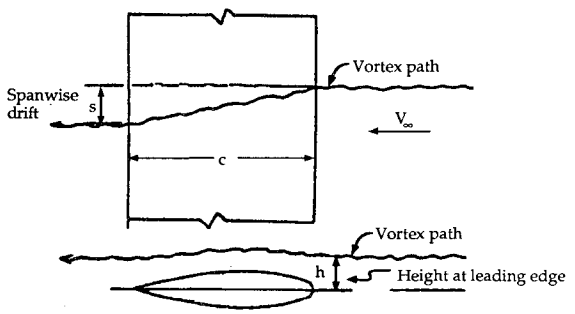

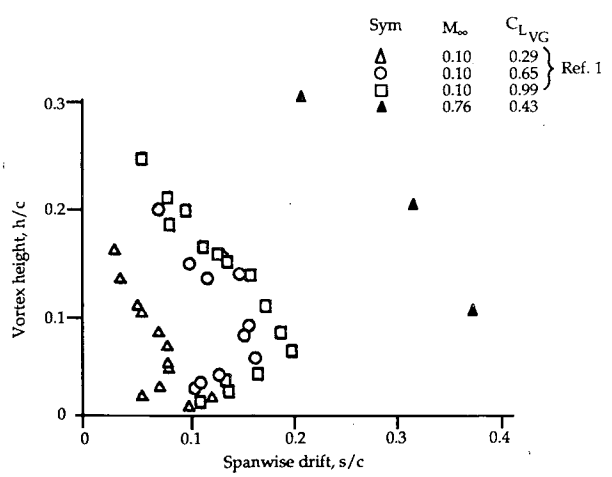

Fig. 19 Spanwise drift of the vortex center.

The contour maps also indicate the appearance of two distinct minimum pressure regions separated by some distance for the intermediate vortex height. The presence of these low pressure regions suggests the possibility of formation of a secondary vortex caused either by the breakup of the primary vortex into two vortices or by formation of secondary vortex caused by the separation of the flow as a result of vortex airfoil interaction (i.e. separation vortex). The secondary vortex, observed for a vortex height of 0.20, is not seen for the closest encounter ($h/c = 0.10$). The exact reason for this is not known at this time. Due to the strong interaction of the vortex with the wake of the downstream airfoil, the secondary vortex might be absorbed within the low pressure region in the wake of the downstream airfoil, and not detectable by the rake pressure measurement alone. Further tests utilizing flow visualization techniques are needed in order to verify such conclusions.

Concluding Remarks

The experimental data obtained from the transonic blade-vortex interaction tests indicate that: 1) the trailing vortex in transonic flows contains a high degree of unsteadiness, particularly near the vortex center; 2) interaction of the vortex with the downstream airfoil substantially alters the pressure distribution of the airfoil. This effect is found to be a function of vortex strength and geometric position of the vortex relative to the downstream airfoil, but is relatively insensitive to the Reynolds number; and 3) the downstream airfoil causes a spanwise drift of the vortex core and the amount of drift tends to increase for cases where the vortex is closer to the airfoil surface.

Acknowledgments

The perpendicular blade-vortex interaction experiments described here came from the study conducted while the first author was a graduate research associate at the University of Texas at Arlington. This work was supported by the U.S. Army Research Office (ARO Grant DAAG29-84-K131).

References

[1]Seath, D. D., and Wilson, D. R., "Vortex-Airfoil Interaction Tests," AIAA 24th Aerospace Sciences Meeting, AIAA Paper 86-0354, Reno, NV, Jan. 6–9, 1986.

[2]Landgrebe, A. J., and Cheney, M. C., Jr., "Rotor Wakes—Key to Performance Predictions," Aerodynamics of Rotary Wings, AGARD CP111, Feb. 1973.

[3]McCroskey, W. J., "Some Current Research on Unsteady Fluid Dynamics," *Transactions of the American Society of Mechanical Engineers, Journal of Fluids Engineering*, Vol. 99, Series 1, No. 1, March 1977, pp. 8–38.

[4]Widnall, S., "Helicopter Noise Due to Blade-Vortex Interaction," *Journal of the Acoustical Society of America*, Vol. 50, No. 1, Pt. 2, 1971, pp. 354–365.

[5]Leighton, K. P., "Research on Model Helicopter Blade Slap at Moderate Tip Speeds," *Journal of the American Helicopter Society*, Vol. 27, No. 3, July 1982, pp. 11–17.

[6]Boxwell, D. A. and Schmitz, F. H., "Full-Scale Measurement of Blade-Vortex Interaction Noise," *Journal of the American Helicopter Society*, Vol. 27, No. 4, Oct. 1982, pp. 11–27.

[7]Srinivasan, G. R., McCroskey, W. J., and Kutler, P., "Numerical Simulation of the Interaction of a Vortex with a Static Airfoil in Transonic Flow," AIAA 22nd Aerospace Sciences Meeting, AIAA Paper 84-0254, Reno, NV, Jan. 9–12, 1984.

[8]George, A. R., "Helicopter Noise: State-of-the-Art," *Journal of Aircraft*, Vol. 15, No. 11, Nov. 1978, pp. 707–715.

[9]George, A. R., and Chang, S. B., "Noise Due to Transonic Blade-Vortex Interactions," 39th Annual Forum of the American Helicopter Society, American Helicopter Society Paper A-83-39-50-D000, Alexandria, VA, 1983.

[10]Leverton, J. W., "Aerodynamics-Historical Prospective and Important Issues," *Proceedings of American Helicopter Society National Specialists' Meeting on Aerodynamics and Aeroacoustics*, American Helicopter Society, Alexandria, VA, 1987.

[11]Leverton, J. W., Pollard, J. C., and Wills, C. R., "Main Rotor Wake-Tail Rotor Interaction," *Vertica*, Vol. 1, No. 3, 1977, pp. 213–221.

[12]Ham, N. D., "Some Conclusions from an Investigation of Blade-Vortex Interaction," *Journal of the American Helicopter Society*, Vol. 20, No. 4, Oct. 1976, pp. 26–31.

[13]Caradonna, F. X., Laub, G. H., and Tung, C., "An Experimental Investigation of the Parallel Blade-Vortex Interaction," Tenth European Rotorcraft Forum, Paper 4, The Hague, The Netherlands, Aug. 1984.

[14]Mandella, M., and Bershader, D., "Qualitative Study of the Compressible Vortex: Generation, Structure and Interaction with Airfoils," AIAA 25th Aerospace Sciences Meeting, AIAA Paper 87-0328, Reno, NV. Jan. 12–15, 1987.

[15]Schlinker, R. H., and Amiet, R. K., "Rotor-Vortex Interaction Noise," AIAA Eighth Aeroacoustics Conference, AIAA Paper 83-0720, Atlanta, GA, April 11–13, 1983.

[16]Phillipe, J. J., and Armand, C., "ONERA Aerodynamic Research on Helicopters," Rotorcraft Design, AGARD CP-233, Jan. 1978.

[17]Wilson, D. R., and Chou, S. Y., "Development of the UTA High Reynolds Number Transonic Wind Tunnel," AIAA 23rd Aerospace Sciences Meeting, AIAA Paper 85-0315, Reno, NV, Jan. 14–17, 1985.

[18]Kalkhoran, I. M., "An Experimental Investigation of the Perpendicular Vortex-Airfoil Interaction at Transonic Speeds," Ph.D. Dissertation, Univ. of Texas, Arlington, TX 1987.

[19]Ohman, L. H., "Experimental Data Base for Computer Program Assessment," AGARD AR-138, May 1979.

[20]Lock, R. C., "Test Cases for Numerical Methods in Two-Dimensional Transonic Flows," AGARD Rept. 575, 1970.

[21]Bertin, J. J., and Smith, M. L., *Aerodynamics for Engineers*, Prentice-Hall, Englewood Cliffs, NJ, 1979.

[22]Patel, M. H., and Hancock, G. J., "Some Experimental Results of the Effect of a Streamwise Vortex on a Two-Dimensional Wing," *Aeronautical Journal*, April 1974, pp. 151–155.